JOURNAL OF GEOPHYSICAL RESEARCH, VOL. ???, XXXX, DOI:10.1029/,

The skill of different ocean tracers in reducing uncertainties about projections of the Atlantic Meridional Overturning Circulation

Marlos Goes* (1), Nathan M. Urban (1), Roman Tonkonojenkov (1),

Murali Haran (2), and Klaus Keller (1,3)

(1) Department of Geosciences, The Pennsylvania State University,

University Park, USA.

(2) Department of Statistics, The Pennsylvania State University,

University Park, USA.

(3) Earth and Environmental Systems Institute,

The Pennsylvania State University, University Park, USA.

* Corresponding author e-mail: mpg14@psu.edu

Submitted to **Journal of Geophysical Research - Oceans**

Friday, August, 21, 2009.

Abstract

The North Atlantic Meridional Overturning Circulation (AMOC) is projected to weaken in response to anthropogenic climate forcings. Quantifying this effect is difficult, however, since the current Earth system models are subject to model biases as well as structural and parametric uncertainties. Observational constraints can help in reducing these uncertainties and therefore constrain projections. Here we analyze and quantify the skill of three different ocean tracers (CFC-11, Δ^{14}C, and temperature data from published datasets) in reducing uncertainties on the parameterization of vertical ocean diffusivity (K_v) and the resulting AMOC projections in an Earth system model of intermediate complexity. Given the model structure and the observational constraints, the Δ^{14}C observations reduce the uncertainty about K_v the most (measured by the reduction of the 95% credible interval), followed by CFC-11 and temperature. The most probable K_v value given the model structure is around 0.2-0.25 cm^{2}s^{-1}. The most likely reduction in AMOC strength between 2000 and 2100 is around 25% under the SRES-A1FI scenario.

1. Introduction

The North Atlantic Overturning Circulation (AMOC) is a key component of the climate system [*Munk & Wunsch*, 1998]. Past changes in the AMOC intensity are associated with considerable changes in global scale temperature and precipitation patterns [*McManus et al.*, 2004]. Anthropogenic climate forcings may trigger an AMOC threshold response, with potentially nontrivial impacts on natural systems and human welfare (*Patwardhan* [2007], *Keller et al.* [2000]). Current AMOC model predictions are deeply uncertain (*Zickfeld et al.* [2007], *Meehl et al.* [2007]).

Tracer observations such as chlorofluorocarbon-11 (CFC-11), or radiocarbon ($\Delta^{14}C$) can provide valuable information to improve estimates of the ventilation rate and advective properties in the ocean [*Doney et al.*, 2004]. Information about such processes is important for evaluating the skill of climate models in simulating the ocean circulation, on time-scales ranging from decadal to centennial. A better representation of these mechanisms can hence improve AMOC projections.

A key parameter for determing ocean circulation properties in models is the vertical ocean diffusivity (K_v), which has a large impact on oceanic heat storage and transport, modeled uptake of ocean tracers such as CO_2 [*Sokolov et al.*, 1998], and it is one of the closure components of the MOC circulation [*Wunsch & Ferrari*, 2004]. This parameter is highly uncertain [*Munk & Wunsch*, 1998], and it is generally tuned in models to generate a realistic AMOC strength. In addition, high model diffusivity can prevent multiple states of the MOC [*Schmittner & Weaver*, 2001].

Several studies (e.g., *England* [1993], *Gao et al.* [1994]) analyzed the importance of the magnitude of the diffusivity strength and parameterization on the MOC structure and representations of tracers in ocean models. These studies, however, are typically silent on the question of how much information is contained in the different types of observations. This is an important question, for example, to inform the design of AMOC observation and prediction systems (cf. *Baehr et al.* [2008], *Keller et al.* [2007]).

Recently, *Schmittner et al.* [2009] applies a relatively simple method to estimate K_v from the combined effects of observation errors and model structural errors. However, their approach neglects the effects of cross-correlation between different tracers, which can generate overconfident probability distributions of climate uncertainties. In another recent study, *Bhat et al.* [2009] estimates the posterior probability distribution for K_v using Δ^{14}C and CFC-11 observations. Their approach uses a Gaussian process emulator for the climate model and estimates the distribution of K_v via a Bayesian approach. While their kernel mixing based approach to constructing the emulator is flexible and efficient, it is conceptually complex and still computationally too demanding for routine use with more than two ocean tracers.

Here we obtain an estimate of the probability distribution of K_v using three tracers simultaneously. Our approach provides a much faster and easier way to implement the methodology, enabling the routine use of information from several ocean tracers jointly, while still considering both spatial autocorrelation and cross-correlation between residuals of different tracers. Furthermore, we advance on previous work by quantifying and ranking the skill of the tracers CFC-11, Δ^{14}C and temperature (T) together from a model calibration to constrain the uncertainties in the model parameter K_v. Our main goal is to apply the joint (all tracers) estimate of the K_v probability density function to improve AMOC predictions.

2. Methods

2.1. Earth System Model of Intermediate Complexity

We use the University of Victoria Earth System Model of Intermediate Complexity (UVic 2.8; *Weaver et al.* [2001]) to produce an ensemble of ten members varying the parameter K_v, the background ocean vertical diffusivity. The K_v values are defined in an equidistant grid, ranging from 0.05–0.5 cm^2s^{-1}. The ocean component in UVic is MOM2 [*Pacanowski*, 1995] with a $1.8° \times 3.6°$ resolution in the horizontal and 19 depth levels. The atmospheric component is a one-layer atmospheric energy-moisture balance model, which does not apply flux correction and is forced by prescribed winds from the NCAR/NCEP climatology. Also included in the model are a thermodynamic sea-ice component, a terrestrial vegetation (TRIFFID) and an oceanic biogeochemistry based on the ecosystem model of *Schmittner et al.* [2005].

The model is spun up from observed data fields as initial conditions for 3000 years (with a coupled carbon cycle for the last 1000 years) for each parameter value. It is then integrated from years 1800-2100 using historical and projected climate forcings (SRES–A1FI scenario), extended to year 2200 following *Zickfeld et al.* [2008]. We modified the model to include non-CO_2 greenhouse gases, volcanic and sulfate forcings from *Sato et al.* [1993] and *Hansen & Sato* [2004]. Atmospheric sulfates follow the same rate of decrease as the CO_2 concentration after 2100.

The model uses the *Gent & McWilliams* [1990] eddy mixing parameterization. It accounts for increased mixing over rough topography based on the tidal mixing scheme of

St. Laurent et al. [2002]. For the Southern Ocean (south of 40S), the vertical mixing is defined as > 1 cm^2/s below 500 meters in order to simulate the more vigorous mixing there (e.g., *Schmittner et al.* [2009], *Matsumoto & Key* [2004]).

2.2. Data

We focus on a subset of three types of observations that have previously been shown (cf. *Schmittner et al.* [2009], *Bhat et al.* [2009], *Toggweiler et al.* [1989]) to provide constraints on the parameterization of K_v in ocean models: (i) temperature (T), (ii) chlorofluorocarbon 11 (CFC-11), and (iii) radiocarbon (Δ^{14}C) observations. Δ^{14}C is defined as the ^{14}C/^{12}C ratio of air-sea fractionation-corrected data [*Stuiver & Polach*, 1977]. Each of the tracers in this subset has a different behavior, and can constrain K_v in different ways. The temperature observations constrain K_v, because K_v affects, for example, the shape of the thermocline as well as the penetration of the anthropogenic heat anomalies [*Gnanadesikan*, 1999]. The Δ^{14}C observations constrain K_v in two main ways, because it has a natural and an anthropogenic component. The natural component can give information of mixing rates (that are, in turn, a function of K_v) in the order of centuries or millennia, while the anthropogenic component, which greatly increased during the 1950s and 1960s due to thermonuclear explosions, provides information on decadal time-scale. The anthropogenic tracer CFC-11 also constrains K_v on decadal time-scale, because atmospheric emissions started in the 1930s. Its solubility in water is dependent on the temperature. Considering CFC-11 and Δ^{14}C jointly can provide new insights into oceanic mixing and K_v because they have very different forcing histories, air-sea equilibration timescales and water solubility (*Broecker & Peng* [1974], *Ito et al.* [2004]), and the observation errors and signal-to-noise ratios of the two tracers are different. We analyze published data products for these three tracers (*Locarnini et al.* [2006]; *Key et al.* [2004]) and average the model hindcasts over the time the observations have been collected, i.e., 1990's for CFC-11 and Δ^{14}C, and 1950-2000 for temperature. The observations were interpolated to the model grid and the model output is restricted to the regions where the data products are available.

Further, we compare the ocean tracers information with the climatological AMOC strength information calculated from observations with the inverse model of *Lumpkin & Speer* [2003], which is estimated as (17.6±2.7 Sv). The model ensemble is calibrated against observations using a Bayesian inference method. We assume a Gaussian likelihood function and estimate the posterior probability of K_v given the observations through a Markov Chain Monte Carlo (MCMC) method [*Metropolis et al.*, 1953]. Our method accounts for auto-correlations of the residuals, as well as cross-correlation between residuals of different tracers. For this, a separable covariance matrix Σ is estimated. The inversion and the numerical implementation of the calibration procedure are detailed in the next subsection. The reader who is not interested in the details of the inversion technique can skip the next subsection without loss of understanding.

2.3. Bayesian model inversion

The goal of Bayesian parameter estimation is to infer a probability distribution $p(\theta|O)$ representing the uncertainty in a climate model parameter θ, conditional on a vector of observed data O. Here θ is the UVic vertical ocean diffusivity parameter K_v. The inferential procedure is based on a statistical model that relates the model parameter (θ) to the observations (O) by way of the ensemble of model output $M(\theta)$. The statistical model used here assumes that the observations are randomly distributed about the model prediction

$$O = M(\theta) + \epsilon\,, \tag{1}$$

where the error is a random variable drawn from a multivariate normal distribution

$$\epsilon \sim N(\mu, \Sigma)\,, \tag{2}$$

with an unknown mean or bias term μ and covariance matrix Σ. These distributional parameters are to be estimated along with the model parameter θ. The error term encompasses all processes which may cause the observations to deviate from the model predictions, including model structural error, natural variability in the climate system, and measurement error. Because these errors are uncertain, they are modeled stochastically as a random process, assumed here to be Gaussian.

The error mean term μ represents model bias which is common across ensemble members. *Schmittner et al.* [2009] assumed a bias which is constant in depth. Here we use a general linear form that varies in depth (z), $\mu = a + bz$, which improves the model fit as indicated by exploratory data analysis. The covariance matrix, described later, captures the residual variability which is not accounted for by the linear bias.

The above probability model describing the spread of observations about the model output defines a likelihood function $L(O|\theta, \mu, \Sigma)$ for the data conditional on the model and covariance parameters:

$$L(O|\theta, \mu, \Sigma) = (2\pi)^{-N/2}|\Sigma|^{-1/2} \exp\left(-\frac{1}{2}\tilde{r}^T\Sigma^{-1}\tilde{r}\right)\,, \tag{3}$$

where Σ is a covariance matrix and $\tilde{r} = O - M(\theta) - \mu$ are the bias-subtracted data-model residuals.

Consider an ensemble M containing p runs of a climate model, where each run corresponds to a different value of the climate model parameter, θ_k, $k = 1, \ldots, p$. For each ensemble member we analyze n ocean tracer profiles defined at d spatial locations (depths). The matrix Σ is $nd \times nd$ specifying the covariance between n tracers at d locations (depths). Assuming separability, Σ can be approximated by a Kronecker product of two matrices:

$$\Sigma = \Sigma_T \otimes C_S + \Sigma_M \,, \tag{4}$$

where Σ_T corresponds to the $n \times n$ cross-covariance matrix of the tracers, and C_S is the $d \times d$ spatial correlation matrix (in depth) respectively. Σ_M is the data measurement error which we assume to be negligible compared to the other errors because of the spatial aggregation of the data.

The cross-covariance matrix Σ_T depends on $n(n-1)/2$ cross-tracer correlation coefficients ρ_{ij} (since ρ_{ij}=ρ_{ji}), and on residual standard deviations σ_i of the n individual tracers:

$$\Sigma_T = \begin{bmatrix} \sigma_1^2 & \sigma_1\sigma_2\rho_{12} & \ldots & \sigma_1\sigma_n\rho_{1n} \\ \sigma_2\sigma_1\rho_{21} & \sigma_2^2 & \ldots & \sigma_2\sigma_n\rho_{2n} \\ \vdots & \vdots & \ddots & \vdots \\ \sigma_n\sigma_1\rho_{n1} & \ldots & \ldots & \sigma_n^2 \end{bmatrix} . \tag{5}$$

We model the spatial correlation C_S using a standard Gaussian correlation function, a special case of the Matérn class of covariance functions (see, for e.g., *Stein* [1999]). This function decays with distance between locations d_i and d_j with a correlation length scale λ, assumed to be the same for all tracers:

$$(C_S)_{ij} = \exp\left(-\frac{|d_i - d_j|^2}{\lambda^2}\right) . \tag{6}$$

Given the property of the Kronecker product (see, for example, *Lu & Zimmerman* [2005]), the multivariate normal likelihood function $L(y, \theta)$ becomes:

$$L(O|\theta, \mu, \Sigma_T, C_S) = (2\pi)^{-N/2}(|\Sigma_T|^d|C_S|^n)^{-1/2} \exp\left[-\frac{1}{2}\tilde{r}^T(\Sigma_T^{-1} \otimes C_S^{-1})\tilde{r}\right] , \tag{7}$$

where $N = nd$ is the total number of data points, and $\tilde{r}$=$[O_1 - M_1 - \mu_1, \ldots, O_n - M_n - \mu_n]^T$ is the concatenated vector containing the misfit between the unbiased model data and respective observations for all tracers. The Kronecker structure of Equation 4 allows the $nd \times nd$ matrix Σ to be efficiently inverted by inverting the two smaller matrices Σ_T $(n \times n)$ and C_S $(d \times d)$.

Once the probability model has been specified in the form of a likelihood function, inference about the posterior distribution of θ is obtained by Bayes' theorem. The theorem states that the posterior probability of the unknown parameters is proportional to their prior probability distribution, multiplied by the likelihood of the data:

$$p(\theta, a, b, \sigma, \rho, \lambda|O) \propto L(O|\theta, a, b, \sigma, \rho, \lambda)\, p(\theta)\, p(a)\, p(b)\, p(\sigma)\, p(\rho)\, p(\lambda) , \tag{8}$$

We draw 20,000 samples from the above posterior distribution by a Markov chain Monte Carlo (MCMC) algorithm. The MCMC algorithm jointly estimates one model parameter $(\theta = K_v)$, $2n$ bias coefficients (a_i and b_i), n standard deviations (σ_i), $n(n-1)/2$ cross-tracer correlations (ρ_{ij}), and one correlation length (λ). This is an improvement upon the methodology of *Schmittner et al.* [2009] which held all parameters but θ fixed at optimized values, and did not consider the uncertainty in the other parameters. Because the model output is only defined on a discrete grid of K_v values, the MCMC algorithm proposes discrete jumps for this parameter during its random walk through parameter space, and continuous moves for all other parameters.

In Equation (8) we assume all parameter priors are independent of each other. We choose a uniform prior $p(\theta)$ for the model parameter K_v. For the correlation length we apply the lognormal prior $\ln\lambda \sim N(5.5, 0.5^2)$, so that the logarithm of λ is normally distributed with mean 5.5 and standard deviation 0.5. This prior locates most of the probability mass of the distribution between 0 and 600 meters. We use Jeffreys priors ($p(\sigma_i) \propto 1/\sigma_i^2$) for the variances, and uniform priors for the bias parameters a_i and b_i. For the cross-covariance matrix we specify an inverse Wishart prior distribution $\Sigma_T \sim IW(S, \nu)$, with a diagonal scale matrix $S = \mathrm{diag}(\sigma_1^2, \ldots, \sigma_n^2)$ and $\nu = 2n+1$ degrees of freedom. A diagonal scale matrix reduces spurious correlations by penalizing tracer residuals which are are not independent of each other. Spurious correlation is not a problem when the data dimension is large, but when the data are sparse such a regularization procedure is prudent.

Equation (8) gives the joint posterior probability of both the model parameter and the bias and covariance parameters. The marginal posterior probability of the model parameter alone is obtained by integrating the joint posterior over all other parameters:

$$p(\theta|O) = \int p(\theta, a, b, \sigma, \rho, \lambda|O)\, da\, db\, d\sigma\, d\rho\, d\lambda\,. \tag{9}$$

Since the posterior is estimated by MCMC sampling, this posterior distribution of θ is easily obtained by simply considering the θ samples while ignoring the samples for the other parameters.

3. Results

The strength of the AMOC in the model is strongly positively correlated with K_v (Figure 1). The model hindcasts of the AMOC strength vary from 8–22 Sv over the considered K_v values. Under the projected anthropogenic climate forcings, the AMOC strength decreases in most cases, but it is more sensitive to the considered forcings for higher K_v values. Due to the strong dependence of the AMOC structure and behavior on the K_v value in this model, a reduction in the K_v uncertainty will produce an improved AMOC hindcast and projection in the model.

Different K_v values result in different hindcasts of CFC-11, $\Delta^{14}C$ and T (Figure 2). In general, the observations are contained by the model ensemble spread. Changing K_v affects the model hindcast of Δ^{14}C differently for surface and for deep waters. Lower K_v values are associated with a lower vertical exchange rate of water from surface to the bottom, decreasing the bottom concentration of Δ^{14}C, and increasing it in the surface. In contrast, higher K_v values result in a stronger exchange of deep waters with generally low Δ^{14}C concentrations to the surface and also increase the rate of deep water mass formation, reducing the surface to bottom Δ^{14}C gradient.

For CFC-11 and T, the highest model errors are located in the deeper portions of the ocean, where the model has generally a lower ventilation rate. This is due to the relatively poor representation of fresh water fluxes in the model, which causes a too stratified isopycnal structure in comparison to observations, and inaccurate representation of the lower North Atlantic Deep Water (NADW) and Antarctic Intermediate Water (AAIW). Both biases are typical for coarse-resolution models (*England* [1993], *Sorensen et al.* [2001]).

Overall, for three types of observations considered, we estimate 14 parameters: K_v, as well as 13 auxiliary parameters (see Section 2.3). As a result, the statistical procedure generates the joint 14-dimensional probability density function (pdf) of the parameters. We focus here first on the marginal projection of this pdf onto the K_v dimension (Figure 3). For comparison, we also show the the climatological AMOC pdf in Figure 3. The K_v pdf is derived from the climatological AMOC estimate of *Lumpkin & Speer* [2003] by assimilating a single data point assuming a normally distributed error. In principle, the model could be calibrated with both the ocean tracer and AMOC strength data by using the derived AMOC pdf as a prior for K_v. However, this would neglect potential correlations between ocean tracer and AMOC strength residual errors. As a proper treatment of AMOC/tracer correlations is beyond the scope of this work, we present the AMOC-derived pdf independently of the pdfs from the ocean tracers.

The three considered sources of information have rather different skill in improving K_v estimates and AMOC predictions (see Table 1 for the properties of the statistical distributions). Δ^{14}C has the highest information content with respect to improving K_v estimates, its posterior 95 % credible interval (CI) is the tightest (0.14 cm^2s^{-1}) in comparison to the other tracers. CFC-11 comes in second, with a 95 % CI of 0.22 cm^2s^{-1}, and T comes last with the largest CI of 0.32 cm^2s^{-1}. All the K_v distributions derived from the tracers information show biases relative to the one estimated from the climatological AMOC strength, with Δ^{14}C containing higher biases toward lower K_v values in comparison to the rest of the tracers. CFC-11 and T show smaller biases than Δ^{14}C compared to the climatological AMOC information. Combining all three sources of information (black curve in Figure 3), the model favors K_v values in the middle of the considered range, from 0.2–0.25 cm^{2}s^{-1}.

As discussed in previous studies (e.g., *Schmittner et al.* [2009]), the K_v value in a coarse resolution ocean model represents the effects of background diffusivity combined with subgridscale diffusivity (i.e., a model shortcoming). Hence, our estimate cannot be directly compared to observed estimates of background diffusivity of 0.1 cm^{2}s^{-1} [*Ledwell et al.*, 1993].

The posterior K_v estimates provide a basis for projections of the AMOC strength in 2100 and 2200 (Figure 4). In 2100, the expected strength for the AMOC in this model is about 10.5 Sv. In 2200 the AMOC shows a slight strengthening relative to the 2100 conditions with an expected value of roughly 11.5 Sv, with a narrower range of projected values.

The magnitude of the estimated cross-correlation terms for the K_v are small, less than 0.4 at the most probable value of K_v (see Table 1). Considering or neglecting the effects of this residual cross correlation does not change drastically the K_v posterior estimate considerably in the analyzed case (results not shown). This can be explained by the relatively good representation of the mean function for the tracers residuals and, as discussed by *Cressie* [1993] (pp. 25), “What is one person’s (spatial) covariance structure may be another person’s mean structure”. In other words, there is a trade-off between estimating a mean function for the tracer residuals to account for structural model errors and the magnitude of the residual cross correlation across the considered sources of information.

4. Conclusion

We develop and apply a method to rank and quantify the skill of different sources of information to reduce the uncertainty about ocean model parameters and the resulting climate predictions. We improve on previous work by (i) refining the estimation of errors in the model structure, (ii) including several ocean tracers at once in a computationally efficient fashion, and (iii) quantifying and ranking the skill of different sources of information to reduce the uncertainty about a model parameter. We demonstrate how Δ^{14}C, CFC-11, and T sharpen the estimates of K_v and improve AMOC projections.

The K_v derived from individual observations (i.e., Δ^{14}C, CFC-11, T) are broadly consistent, but show slight discrepancies that we attribute predominantly to structural model errors. Of the considered observations, Δ^{14}C has the highest skill in reducing uncertainties in AMOC projections, but in this model it has also the highest bias. $\Delta^{14}C$ is followed (in decreasing skill of being able to reduce K_v uncertainty) by CFC-11 and T.

AMOC projections show a reduction of the maximum of the joint posterior in 2100 by roughly 25% (3.5 Sv). It is perhaps both surprising and encouraging that the pdf of K_v estimated in this study based on CFC-11, T, Δ^{14}C is remarkably similar to the estimate of *Bhat et al.* [2009], which uses only CFC-11 and Δ^{14}C, a much more computationally complex method, and a slightly different representation of ocean biogeochemical fluxes, mixing in the Southern Ocean, and anthropogenic emissions. This convergence of K_v estimates based on different combinations of considered sources of information and statistical methods might suggest that K_v can be robustly estimated from the oceanic tracers studied here.

Our results are subject to many caveats. These caveats point to potentially fruitful research directions. First, we consider only highly aggregated data. Basinwide zonal averages could, for example, provide potentially useful information about where the model performs better. Second, other model parameters, such as climate sensitivity or sensitivity of climate to aerosol concentrations, (cf. *Tomassini et al.* [2007] and *Forest et al.* [2002]), are also highly uncertain and impact AMOC projections as well.

Acknowledgments. We thank Mike Eby, Andreas Schmittner, Damon Matthews, Bob Key and Ray Najjar for helpful discussions and feedback. This work is partially supported by the National Science Foundation as well as by the U.S. Department of Energy's Office of Science (BER) through the Northeastern Regional Center of the National Institute for Climatic Change Research. Any errors and opinions are those of the authors alone.

References

Baehr, J., D. McInerney, K. Keller, and J. Marotzke (2008), Optimization of an observing system design for the North Atlantic meridional overturning circulation, *J. of Atmos. and Ocean. Tech.*, **25**, 625–634.

Bhat, K.S., Haran, M., Tonkonojenkov, R., and Keller, K. (2009), Inferring likelihoods and climate system characteristics from climate models and multiple tracers. *Annals of Applied Statistics.*, *in review*. Available at http:/www.geosc.psu.edu/∼kkeller.

Broecker, W.S., and T.H. Peng (1987), Gas exchange rates between air and sea. *Tellus*, **26**, 21–35.

Bryan, F. O., G. Danabasoglu, P. R. Gent, and K. Lindsay (2006), Changes in ocean ventilation during the 21st century in the CCSM3. *Ocean Model.*, **15**, 141–156.

Cressie, N.A. (1993), Statistics for Spatial Data, Wiley, New York, 900 pp.

Danabasoglu, G., J. C. McWilliams, and P. R. Gent, (1994), The role of mesoscale tracer transports in the global ocean circulation. *Science*, **264**, 1123–1126.

Doney et al. (2004), Evaluating global ocean carbon models The importance of realistic physics. *Glob. Biogeochem. Cycles*, **18**, GB3017, doi:10.1029/2003GB002150.

England, M. H. (1993), Representing the global-scale water masses in ocean general circulation models. *J. Phys. Oceanogr.*, **23**, 1523–1552.

Chris E. Forest, Peter H. Stone, Andrei P. Sokolov, Myles R. Allen, and Mort D. Webster (2002), Quantifying Uncertainties in Climate System Properties with the Use of Recent Climate Observations. *Science*, **295** (5552), 113. [DOI: 10.1126/science.1064419].

Gao, Y., H. Drange, and M. Bentsen (2003), Effects of diapycnal and isopycnal mixing on the ventilation of CFCs in the North Atlantic in an isopycnic coordinate OGCM.

Tellus, **55B**, 837–854.

Gent, P. R., and J. C. McWilliams (1990), Isopycnal mixing in ocean circulation models. *J. Phys. Oceanogr.*, **20**, 150–155.

Gent, P. R., F. O. Bryan, G. Danabasoglu, K. Lindsay, D. Tsumune, M. W, Hecht, and S. C. Doney (2006), Ocean Chlorofluorocarbon and Heat Uptake during the Twentieth Century in the CCSM3. *J. Climate*, **19**, 2366–2381.

Gnanadesikan, A. (1999), A simple predictive model for the structure of the oceanic pycnocline. *Science*, **283**, 2077–2079.

Hansen, J., and M. Sato (2004), Greenhouse gas growth rates. *Proc. Natl. Acad. Sci.*, USA 101, 16109–16114.

Ito, T., J. Marshall, and M. Follows (2004), What controls the uptake of transient tracers in the Southern Ocean? *Glob. Biogeochem. Cycles*, **18**, GB2021, doi:10.1029/2003GB002103.

Keller, K., Tan, K., Morel, F.M.M. and Bradford, D.F. (2000), 'Preserving the ocean circulation: Implications for climate policy'. *Climatic Change*, **47**, 17–43.

Keller, K., C. Deutsch, M. G. Hall and D. F. Bradford (2007), Early detection of changes in the North Atlantic meridional overturning circulation: Implications for the design of ocean observation systems. *J. Climate*, **20**, 145–157.

Key, R.M., A. Kozyr, C.L. Sabine, K. Lee, R. Wanninkhof, J. Bullister, R.A. Feely, F. Millero, C. Mordy, T.-H. Peng (2004), A global ocean carbon climatology: Results from Global Data Analysis Project (GLODAP). *Glob. Biogeochem. Cycles*, **18**(4), GB4031, doi: 10.1029/2004GB002247.

Ledwell, J. R., A. J. Watson, and C. S. Law (1993), Evidence for slow mixing across the pycnocline from an open-ocean tracer-release experiment. *Nature*, **364**, 701–703.

Locarnini, R. A., A. V. Mishonov, J. Antonov, T. Boyer, and H. E. Garcia (2006), World Ocean Atlas 2005. Volume **1**: Temperature, 182 pp, U.S. Government Printing Office, Washington, D.C.

Lu, Nelson and Zimmerman, Dale L. (2005), The likelihood ratio test for a separable covariance matrix. *Stat. & Prob. Lett.*, **73**(4), 449–457

Lumpkin, R. and K. Speer (2003), Large-scale vertical and horizontal circulation in the North Atlantic Ocean. *J. of Phys. Oceanogr.*, **33**(9), 1902–1920.

Matsumoto, K. and R. M. Key (2004), Natural Radiocarbon Distribution in the Deep Ocean. *Global Environmental Change in the Ocean and on Land*, Eds., M. Shiyomi et al., pp. 45–58.

McManus, J.F., Francois, R., Gherardi, J.M., Keigwin, L.D. and Brown-Leger, S. (2004), Collapse and rapid resumption of Atlantic meridional circulation linked to deglacial climate changes. *Nature*, **428**, 834–837.

Meehl, G.H., T.F. Stocker, W.D. Collins, P. Friedlingstein, A.T. Gaye, J.M. Gregory, A. Kito, R. Knutti, J.M. Murphy, A. Noda, S.C.B. Raper, I.G. Watterson, A.J. Weaver and Z.-C. Zhao (2007), Global climate projections. *Climate Change 2007: The Physical Science Basis*. Contribution of Working Group I to the Fourth Assessment Report of the Intergovernmental Panel on Climate Change, S. Solomon, D. Qin, M. Manning, Z. Chen, M. Marquis, K.B. Averyt, M. Tignor and H.L. Miller, Eds., Cambridge University Press, Cambridge, 747–846.

Metropolis, N., A.W. Rosenbluth, M.N. Rosenbluth, A. H. Teller and E. Teller (1953), Equation of state calculations by fast computing machines. *J. of Chem. Phys.*, **21**, 1087–1092.

Munk W. and Wunsch, C. (1998), Abyssal Recipes-II: Energetics of Tidal and Wind Mixing. *Deep Sea Res.*, **13**, 1977–2010

Pacanowski, R.C. (1995), MOM 2 documentation: Users guide and reference manual, Version 1.0. GFDL Ocean Group Technical Report No. 3, Geophysical Fluid Dynamics Laboratory, Princeton, New Jersey.

Patwardhan, A., S. Semenov, S. Schneider, I. Burton, C. Magadza, M. Oppenheimer, B. Pittock, A. Rahman, J. Smith, A. Suarez, F. Yamin, K. Keller, A Todorov, A. Finkel, D. MacMynowski, M. Mastrandrea, M. Fuessel, J. Corfee-Morlot, R. Sukumar, J.-P. van Ypersele, and J. Zillman (2007), Assessing key vulnerabilities and the risk from climate change, Chapter 19 in the Intergovernmental Panel on Climate Change Fourth Assessment Report, Working group II: Impacts, Adaptation and Vulnerability, Cambridge University Press.

Sato, M., J.E. Hansen, M.P. McCormick, and J.B. Pollack (1993), Stratospheric aerosol optical depth, 1850–1990. *J. Geophys. Res.*, **98**, 22987–22994.

Schmittner, A., N.M. Urban, K. Keller, and D. Matthews (2009), Using tracer observations to reduce the uncertainty of ocean diapycnal mixing and climate carbon-cycle projections. *Global Bio. Cycles.*, in press, available at http:/www.geosc.psu.edu/∼kkeller.

Schmittner, and A. J. Weaver (2001), Dependence of multiple climate states on ocean mixing parameters. *Geophys. Res. Lett.,* **28**, 1027–1030.

Schmittner, A., A. Oschlies, X. Giraud, M. Eby, and H. L. Simmons (2005), A global model of the marine ecosystem for long-term simulations: Sensitivity to ocean mixing, buoyancy forcing, particle sinking, and dissolved organic matter cycling. *Glob. Biogeochem. Cycles*, **19**(3), GB3004, doi: 10.1029/2004GB002283.

Sokolov, A., C. Wang, G. Holian, P. Stone, and R. Prinn (1998), Uncertainty in the oceanic heat and carbon uptake and its impact on climate projections. *Geophys. Res. Lett.*, **25**, 3603–3606.

Sorensen, J., J. Ribbe, and G. Shaffer (2001), Antarctic intermediate water mass formation in ocean general circulation models. *J. Phys. Oceanogr.*, **31**, 3295–3311.

Stein, Michael Leonard (1999), Interpolation of Spatial Data: Some Theory for Kriging, Springer-Verlag Inc., 247 pp.

St. Laurent, L., H. L. Simmons, S. R. Jayne (2002), Estimating tidally driven mixing in the deep ocean. *Geophys. Res. Lett.,* , **29**, 2106–2110, doi:10.1029/2002GL015633.

Stuiver, M. & Polach, H.A (1977), "Discussion: Reporting of 14 C data", Radiocarbon, **19**, no. 3, pp. 355–363.

Toggweiler, J.R., Dixon, K., and Bryan, K. (1989), Simulations of radio–carbon in a coarse–resolution, world ocean model, II. Distributions of bomb–produced ^{14}C. *J. Geophys. Res.*, 94, 82438264.

Tomassini, L., P. Reichert, R. Knutti, T. F. Stocker and M. Borsuk (2007), Robust Bayesian uncertainty analysis of climate system properties using Markov chain Monte Carlo methods, *Journal of Climate*, **20**, 1239–1254.

Weaver, A.J., M. Eby, E. C. Wiebe, C. M. Bitz, P. B. Duffy, T. L. Ewen, A. F. Fanning, M. M. Holland, A. MacFadyen, H.D. Matthews, K.J. Meissner, O. Saenko, A. Schmittner, H. Wang and M. Yoshimori (2001), The UVic Earth System Climate Model: Model description, climatology, and applications to past, present and future climates. *Atmosphere-Ocean*, **39**(4), 361–428.

Wunsch, C., and R. Ferrari (2004), Vertical Mixing, Energy, and the General Circulation of the Oceans. *Ann. Rev. Fluid Mech.*, **36**, 281–314.

Zickfeld, K., A. Levermann, M. Morgan, T. Kuhlbrodt, S. Rahmstorf, and D. Keith (2007), Expert judgements on the response of the Atlantic meridional overturning circulation to climate change. *Climatic Change*, **82**, 235–265

Zickfeld, K., M. Eby, and A.J. Weaver (2008), Carbon-cycle feedbacks of changes in the Atlantic meridional overturning circulation under future atmospheric CO2. *Glob. Biogeochem. Cycles*, **22**, GB3024, doi:10.1029/2007GB003118.

List of Figure Captions

Figure 1. AMOC strength (Sv), defined as the maximum of the transport stream function in the North Atlantic, for the ensemble members from years 1800 to 2200. The gray patch represents the mean ± 1 σ of the estimate provided by *Lumpkin & Speer* [2003].

Figure 2. Global averaged profiles of CFC-11 [*Key et al.*, 2004], Δ^{14}C [*Key et al.*, 2004] and T [*Locarnini et al.*, 2006], for the observations (gray dots) and model ensemble (colored lines). The legend for the model K_v values is the same as in Figure 1.

Figure 3. Posterior probability density function for all considered sources of information (colored lines), the joint posterior using all available observations (black line), and the climatological AMOC estimate [*Lumpkin & Speer*, 2003] for comparison (magenta triangles). The grey triangles on the top are the location of the samples of K_v in the model ensemble.

Figure 4. Joint posterior probability density function for the AMOC using the three considered tracers for the years 2000, 2100 and 2200.

Table 1. Properties of the statistical distributions (mean (cm^2s^{-1}), mode (cm^2s^{-1}) and 95% credible interval [CI] (cm^2s^{-1})) of K_v for each considered sources of information, the posterior (joint distribution considering all tracers information), and the climatological AMOC estimate (*Lumpkin & Speer* [2003]). Also shown are the cross-tracers correlation at the best K_v value estimated in the joint posterior.

Observation	Mode	Mean (cm^2s^{-1})	95% CI	Cross-corr. at best K_v		
				$\Delta^{14}C$	CFC-11	T
$\Delta^{14}C$	0.15	0.16	0.14	1	0.38	-0.16
CFC-11	0.25	0.26	0.22	–	1	0.028
T	0.25	0.25	0.32	–	–	1
posterior	0.20	0.21	0.12	–	–	-
AMOC clim	0.35	0.34	0.33	–	–	-

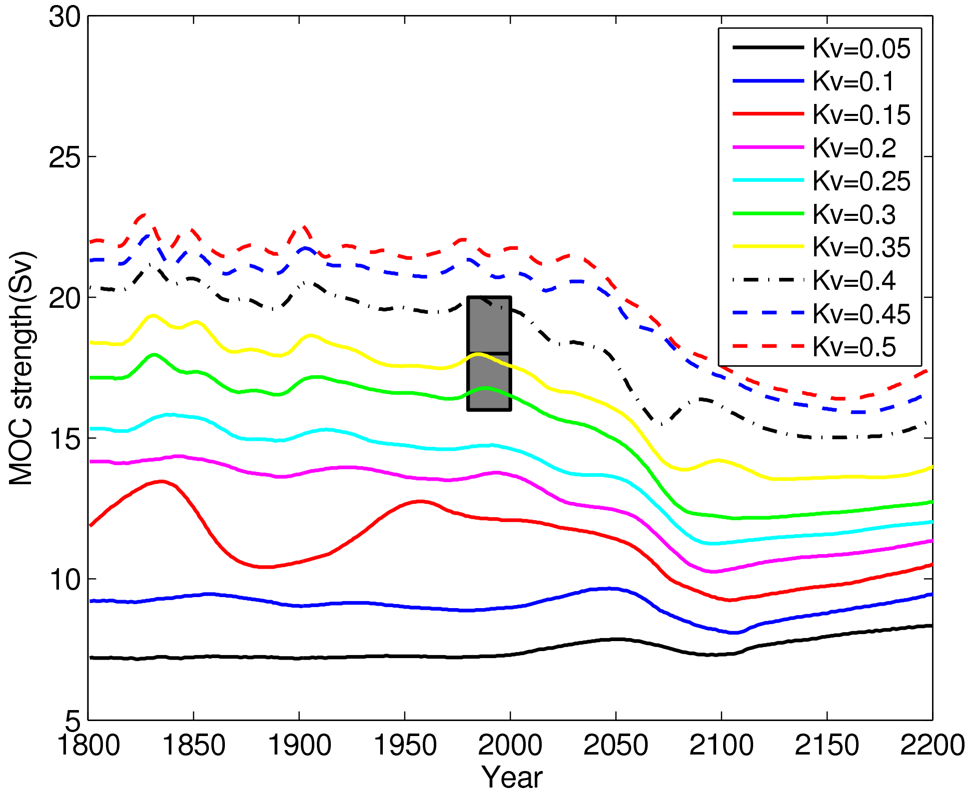

Figure 1. AMOC strength (Sv), defined as the maximum of the transport stream function in the North Atlantic, for the ensemble members from years 1800 to 2200. The gray patch represents the mean $\pm$ 1 σ of the estimate provided by *Lumpkin & Speer* [2003].

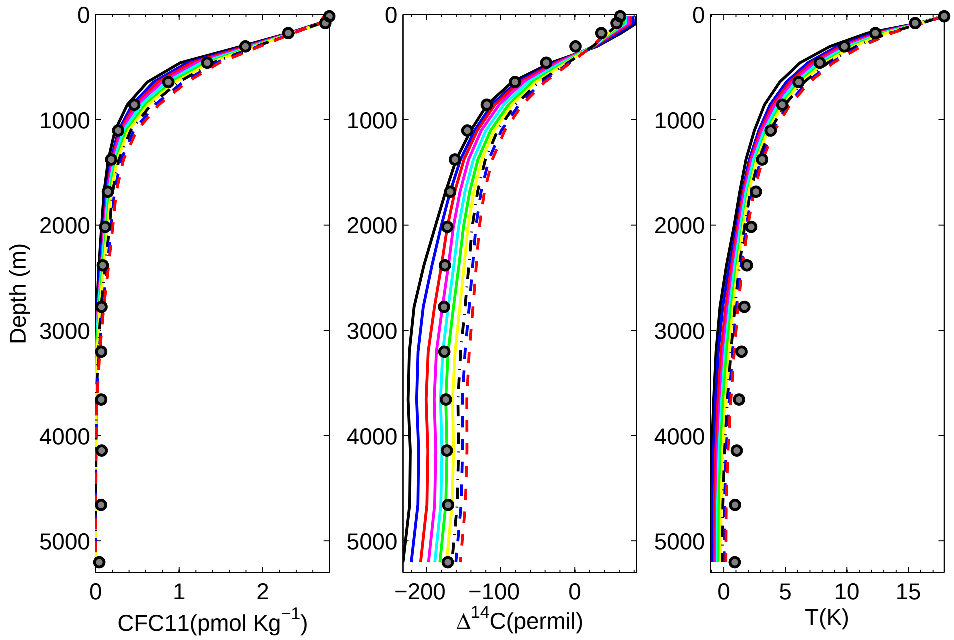

Figure 2. Global averaged profiles of CFC-11 [*Key et al.*, 2004], Δ^{14}C [*Key et al.*, 2004] and T [*Locarnini et al.*, 2006], for the observations (gray dots) and model ensemble (colored lines). The legend for the model K_v values is the same as in Figure 1.

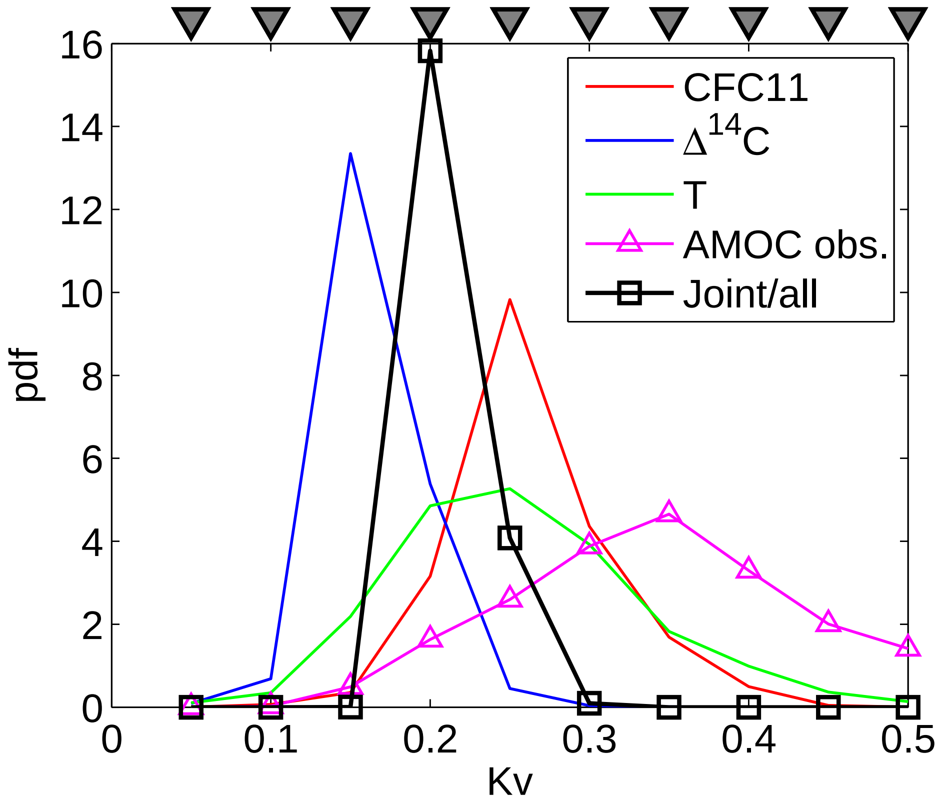

Figure 3. Posterior probability density function for all considered sources of information (colored lines), the joint posterior using all available observations (black line), and the climatological AMOC estimate (*Lumpkin & Speer* [2003]) for comparison (magenta triangles). The grey triangles on the top are the location of the samples of K_v in the model ensemble.

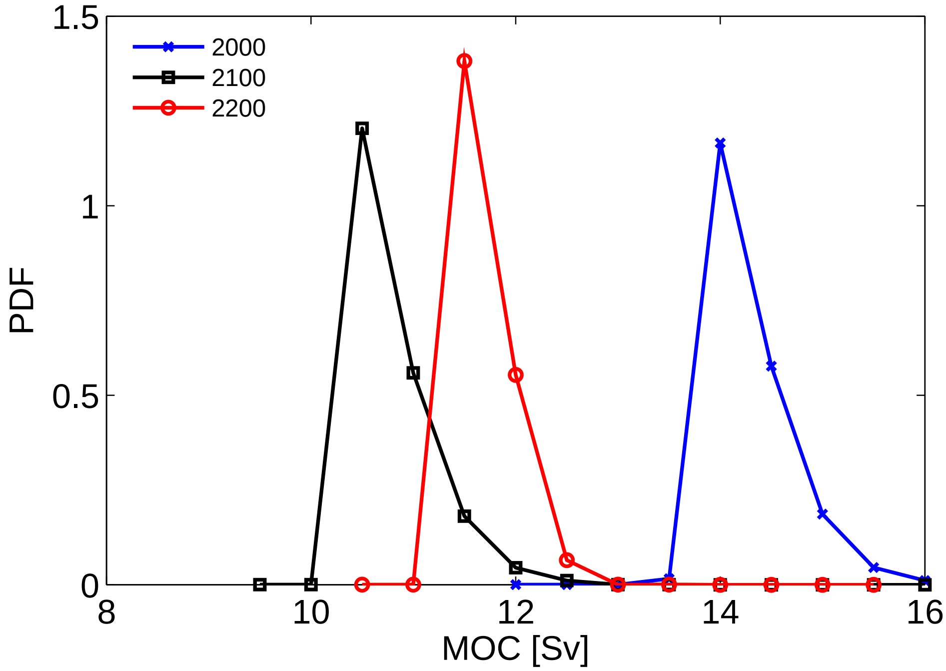

Figure 4. Joint posterior probability density function for the AMOC using the three considered tracers for the years 2000, 2100 and 2200.